Industrial Electrical Engineering and Automation

Coordinated Control of HVDC Links for Damping of Electro-mechanical Oscillations

Samuel Thomasson

Dept. of Industrial Electrical Engineering and Automation

Lund University

Abstract

Due to the deregulation of the Nordic power market, the transmission capacity demands for the power lines are increasing. It is therefore interesting to study bottlenecks, i.e. a shortage of transmission capability. The pair of 420 kV power lines at Hasle connecting Sweden and Norway near Oslo is considered a bottleneck. To improve this situation, an increase in the power transfer limit is desired. Since the transfer limit at Hasle is constrained by insufficient damping of electro-mechanical oscillations, additional damping is of interest.

Coordinated control of two HVDC links are suggested for this increase. To increase the damping by using one HVDC link is a proven method, but the use of two HVDC links in series for this purpose has not been tried before.

A model of the Nordic power system is used to investigate the effectiveness of the solution. Simulations carried out in Eurostag show that the solution works - the damping is improved in all cases tested here and thus the power transfer capacity at Hasle is increased. The damping for the worst case, a bolted three phase short circuit at one of the Hasle lines, was improved from –2% to 3% using ±50 MW of damping power. The voltage variations in Denmark for this case were ±12 kV.

Acknowledgements

Abbreviations

HVDC   High Voltage Direct Current
IGBT   Insulated Gate Bipolar Transistor
SINTEF   The Foundation for Scientific and Industrial Research at the Norwegian Institute of Technology (NTH)
POD   Power Oscillation Damper

Definitions

AC source

e_a line-to-neutral voltage phase a
e_b line-to-neutral voltage phase b
e_c line-to-neutral voltage phase c
L_c AC source inductance

HVDC

V_{d0} Ideal no-load direct voltage
$V_{d0r,i}$ Ideal no-load direct voltage at the rectifier (r) or inverter (i)
V_d Average direct voltage
I_d Direct current
R_c Commutating resistance
$R_{cr,i}$ Commutating resistance at the rectifier (r) or inverter (i)
R_L DC line resistance

Rectifier
α Ignition delay angle
μ Overlap angle
δ Extinction delay angle $(\alpha+\mu)$

Inverter
γ Extinction advance angle
μ Overlap angle
β Ignition advance angle $(\gamma+\mu)$

Oscillations

Tie lines

P   Active power flow on a tie line

V_1 Voltage at one end of a tie line

V_2 Voltage at the other end of a tie line

X   Line reactance

θ_1 Voltage angle at the end of a tie line

θ_2 Voltage angle at the other end of a tie line

Synchronous machines

T_a Accelerating torque

T_m Mechanical torque

T_e Electrical torque

δ Angular position of the machine rotor

ω_0 Nominal synchronous speed (100π rad.)

H   Inertia constant

P_m Mechanical power

P_e Electrical power

Modal analysis

λ Eigenvalue ($\sigma \pm j\omega$)

σ Damping

ω Oscillation frequency in rad/s

f   Frequency in Hz

ζ Damping ratio

Table of Contents

1   INTRODUCTION

This chapter constitutes an introduction to the thesis. The contents and goals of this work are described.

1.1   The Nordic power system

The Nordic power system consists of the combined power systems in Sweden, Norway, Denmark and Finland. The installed capacity is 90,876 MW, the maximum available production capacity is 71,970 MW and the highest recorded peak load has been 67,791 MW. In 2004, almost 75% of this energy came from hydro and nuclear facilities [1].

See figure 1 on the next page for a detailed view of the Nordic transmission grid. The location of Hasle and the HVDC links are indicated.

1.2   Contents of this thesis

In chapter two, power system stability is discussed. Damping and modal analysis are also mentioned. Chapter three is an introduction to HVDC theory. This chapter deals with the main components of an HVDC system and also the damping controller.

Chapter 4 presents various aspects of the simulation model such as purpose and complexity. Chapter 5 shows the simulation results. The results are also discussed in this chapter.

Finally, some suggestions for future work are mentioned in chapter 6.

Figure 1.　　　The Nordic transmission grid [2]

1.3   Goals

Due to the deregulation of the Nordic power market and increasing loads, the demands placed on the power lines are increasing [3, 4]. To be able to safely operate the power system at these new higher power levels, reinforcements to the Nordic grid are being planned [5]. This work focuses on increasing the power transfer limit of the two 420 kV power lines at the Hasle corridor (see figure 1). At present, their power transfer capacity is limited by inadequate damping of electro-mechanical oscillations between Norway and Sweden [3, 6].

HVDC links with damping controllers is a good choice due to the fact that HVDC links at good locations are already built, so only the damping controllers need to be installed. Second, HVDC is a very powerful tool when increasing the damping of oscillations. It has been used before with good results, which makes it even more attractive. The reason to investigate the present case further is that two links are used together, whereas to our knowledge only single links has been utilized for damping purposes so far.

The HVDC links utilized to increase the damping at Hasle are *Konti-Skan* and *Skagerrack*. *Konti-Skan* connects Sweden and Denmark by a pair of submarine DC power cables with a total capacity of 250 + 300 = 550 MW. *Skagerrack* connects Denmark and Norway by three submarine DC power cables with a total capacity of 440 + 500 = 940 MW [7].

To be able to study the effects of installing the damping controller (or POD, power oscillation damper), a model of the Nordic power system consisting of 22 generators and 41 buses is simulated using Eurostag. By simulating, it can be determined how good the suggested solution works. Then, to get a more exact comparison, the damping of the mode before and after the POD is installed is compared.

2 POWER SYSTEM STABILITY

Power system stability is an important part of any power system. The type of stability issue that is relevant for the thesis is explained. Modal analysis is also mentioned.

2.1 Introduction to the stability problem

Power lines obviously have thermal loading limits, but there are also stability limits that must be adhered to. Inadequate damping of oscillations sets one such limit.

Heavily loaded power lines reduce the damping of oscillations [8]. This can reduce the highest allowable power transfer to a level that is lower than the thermal power transfer limit since low and especially negative damping is not acceptable.

The power transfer limit at Hasle is limited by low damping of an interarea mode oscillation at 0.54 Hz (0.58 Hz with both Hasle lines in service, 0.54 Hz with one Hasle line in service) [3, 6]. Interarea oscillations are a case of small-signal stability [9].

A power system is small-signal stable if its generators can remain in synchronism (in phase with each other) after a small disturbance has occurred. Examples of small disturbances are the small load and generation changes that continually take place in a power system. These changes are considered small enough that a linearization of the non-linear power system equations is valid. Instability in this case is the result of either a lack of synchronizing torque or damping torque in the synchronous machine (generator or motor). In the former the result is a steady increase of the rotor angle, in the latter the result will be oscillations of increasing amplitude.

The small-signal analysis does not take the non-linear behavior during large events into account since it is only valid around the linearized operating point. This is why time domain simulations (transient stability analysis) are a good complement to small-signal analysis [10]. In this case, the generators must remain in synchronism after a massive transient disturbance has occurred, e.g. a low impedance short circuit on the 420 kV level or a generator shut down. Here, the non-linear equations governing the power system must be used. A linearized model is not valid during these kinds of events.
The stability of the system depends both on its initial state and on the severity of the disturbance [9].

2.2   Damping

The damping needs to be good at both steady state and during a transient disturbance. If not, even very small disturbances can create large oscillations or instability results when the system is subjected to a large disturbance, respectively.

The following properties increase the effects of disturbances:

1. Heavily loaded power lines will decrease the damping [8]
2. Varying generator inertia can make the rotation speeds of the generator shafts change differently during a fault [7]
3. Different distances to the fault can have the same effect as point two above
4. Incorrectly tuned control systems [13]

2.3   Oscillations

To gain some insight into power system oscillations, an analogy with masses and springs can be useful [11]. See figure 2 below.
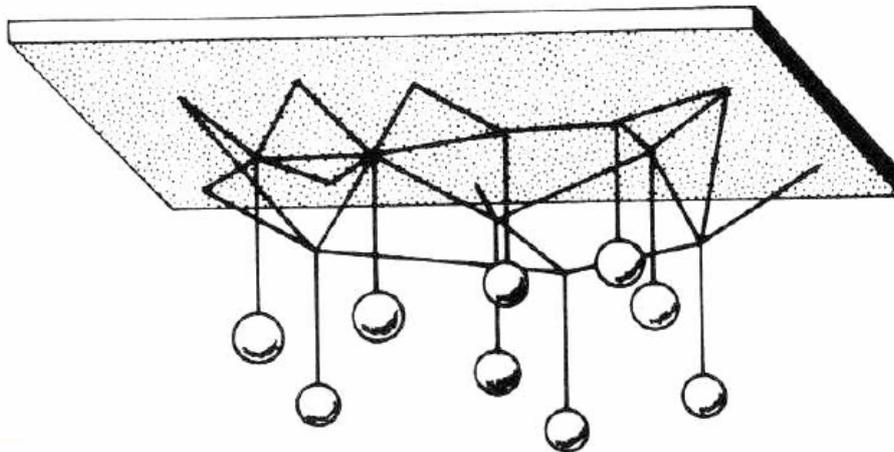

Figure 2.   Mechanical analogy [12]

A large generator inertia will be represented by a large mass, and a strong power line is represented by a spring with a large spring constant. By using this analogy, it is now easy to see that if one or more of the masses are set in motion, that motion has the potential to affect the entire power system. If the resulting disturbance is severe, the forces acting on the springs will be too high, causing them to snap. In a power system this event corresponds to a line tripping which makes the power system more vulnerable

to further faults.

It can also be seen that springs with large spring constants make generators couple much better than springs with low spring constants. When large groups of closely coupled generators swing against another group across weak lines, an interarea oscillation is created. Increased power transfers now result across the weaker power lines such as Hasle due to the relative changes in the generator rotor angles of the closely coupled generator groups. This is the kind of oscillation this work deals with.

The following part explains why oscillations are created.

Two generators (synchronous machines) are connected through a tie line. The active power through that tie line can be expressed as

$$P = \frac{V_1 V_2}{X} \sin(\theta_1 - \theta_2)$$

X is the line reactance, V_1 and V_2 are the voltage magnitudes and θ_1 and θ_2 are the phase angles of the line voltages at each end.

When a fault occurs on the tie line, the active generator power is reduced according to the formula above due to the voltage drop at the fault. As a consequence the rpm of the machines increase. Properties two and three shown in chapter 2.2 explain why one machine can have a relatively higher rpm than the other.

The equation below shows how the accelerating torque T_a of a synchronous machine changes when either the mechanical torque or the electrical torque changes [9].

$$T_a = T_m - T_e$$

This can also be expressed in terms of rotor angle change as [9]

$$\frac{d^2 \delta}{dt^2} = \frac{\omega_0}{2H} \left(P_m - P_e \right)$$

Here, ω_0 is the synchronous speed, H is the inertia constant of the generator, P_m is the mechanical power and P_e is the electrical power.

If one of the machines rotates faster than the other, the faster machine gets a portion of the load from the slower machine due to its increased rpm, slowing it down. Also, its angular position acceleration for the faster machine alters the power transfer through the tie line according to the tie line power formula on the top of this page. Due to the low damping the machines do not reach steady state immediately, but after an oscillation.

If the angular difference θ_1-θ_2 gets beyond a critical value, an increase of it leads to a decrease in power transfer, leading to an even larger difference. This inevitably leads to instability (transient angle instability) [9].

In the case of a generator at one end and a load at the other end, the critical value of power transfer is when a decrease in the load impedance leads to a decrease in active load power. Any ventures beyond this value also inevitably lead to instability (voltage instability) [9].

In the case of incorrectly tuned control systems, the fault does not need to be large at all to create blackouts. If the damping is negative from the start, relatively small events can create blackouts since the system is already unstable.

If the damping is good, however, the stability limits are higher. The maximum power transfer level is now higher and the power system can withstand greater disturbances, provided that the thermal capabilities of the power lines are not exceeded.

It is therefore important to keep the damping as high as possible. The n-1 criterion that is used in the Nordic power system says that one main item (e.g. a transformer, a power line, a generator), must be able to be tripped without a blackout occurring somewhere [14]. This is considered a good compromise between stability and cost.

2.4   Modal analysis

Modal analysis is used to find out the modes (dynamics) of a linear system. A mode is made up of a frequency and its damping [11]. Each mode has either real or complex eigenvalues. Real eigenvalues are non-oscillatory and complex ones (pairs) are oscillatory [9]. Depending on the location of the eigenvalues on the real axis, the damping of the mode can be either positive, zero or negative. Obviously, the two latter are not wanted in a power system.

An interarea oscillation has complex eigenvalues that have the following form [9]:

$$\lambda = \sigma \pm j\omega$$

σ determines the damping and ω determines the oscillation frequency in rad/s.
The more negative σ is, the better damped that mode is. If it is zero, that mode exhibits zero damping. A positive value corresponds to an oscillation with negative damping.

The oscillation frequency expressed in Hz instead of rad/s is equal to [9]

$$f = \frac{\omega}{2\pi}$$

The damping ratio for a mode is determined by [9]

$$\zeta = -\frac{\sigma}{\sqrt{\sigma^2 + \omega^2}}$$

Since the oscillation frequencies in power systems can vary from tenths to tens of Hz it is better to compare damping ratios than time constants. With equal time constants, the number of oscillation cycles needed to reach a certain level varies with the oscillation frequency. However, with equal damping ratios, the number of oscillation cycles needed to reach a certain level is the same, regardless of oscillation frequency [13]. This makes it easier to compare different modes.

3   HVDC THEORY

This chapter describes the components that comprise the HVDC system, from the thyristor valves to the damping controller.

3.1   Main HVDC components

An HVDC system consists of the following main components, as seen in figure 3:
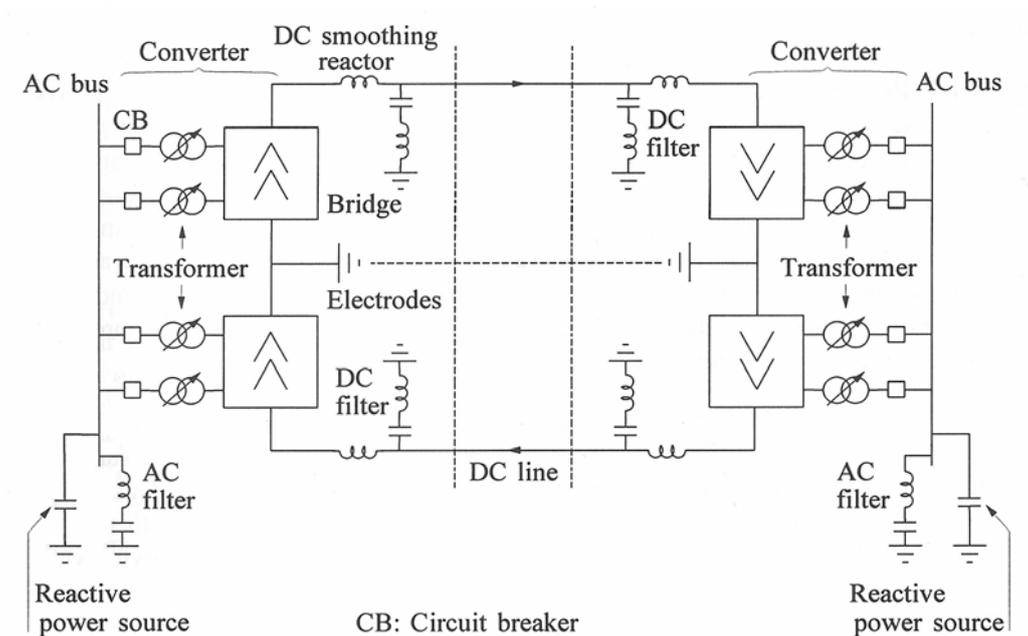
Figure 3.   Main components of an HVDC system [9]

The components are:

- Converter (bridges and transformers),
- DC lines,
- DC filters,
- DC smoothing reactors
- reactive power compensation, and
- a control system

The converter can operate either as a rectifier or an inverter. A rectifier converts AC to DC and an inverter converts DC to AC. Transformers with tap changers are also connected between the AC side and the converter, serving as input and output voltage changers. Depending on the required level of DC voltage and harmonics, more than one transformer per converter can be used.

Each transformer is connected to a three-phase bridge. This creates a 6-pulse converter. It is the number of pulses on the DC side per cycle of AC that determines the pulse number.

Two bridges can be connected in series to increase the DC voltage and reduce the ripple. In this case, a Y-Δ transformer is connected to one bridge and a Y-Y transformer is connected to the other bridge. This creates DC ripple pulses that are 30° apart instead of 60°, which reduce the ripple amplitude and harmonics. With 12 pulses per cycle, this is called a 12-pulse converter. Higher pulse numbers also exist which create even less amounts of DC ripple. However, since they are more complicated than their 12-pulse counterparts, a more practical solution is to use 12-pulse converters and more filtering [9].

In its easiest form, a 12-pulse converter is made up of twelve valves. In reality, though, a lot more valves are used due to the high voltages used in HVDC [7]. *Konti-Skan II* uses 576 water-cooled thyristors per converter in a 12-pulse configuration [15]. Mercury-arc valves are used in earlier HVDC converters, thyristors are used in systems from mid-1970s and IGBTs are used in HVDC light. Both Konti-Skan and Skagerrack use thyristor valves. Konti-Skan used to have mercury-arc valves but they were replaced by thyristors in 2006 [7].

A thyristor acts as a switch that is controlled by the gate. When a positive voltage is applied to the gate, the valve begins to conduct if the voltage potential at the anode is higher than at the cathode. It stops conducting when the current drops to zero and a reverse voltage bias is applied. The valve is now blocking and no current is conducted until a gate pulse is applied when the anode is positive relative to the cathode [9]. The difference between thyristors and IGBTs in this respect is that the current trough IGBTs can be turned off at will.

DC lines are similar to AC lines except for the number of conductors and required spacing. The total cross-section area used for the *Konti-Skan I* submarine cables on the Danish side is 930 mm^2. The conductor material is copper [15].

Smoothing reactors are used to further reduce DC harmonics and to limit the short circuit current if a fault occurs on the DC line. They also prevent discontinuous DC current during light load. This inductance is 0.6 H for *Konti-Skan I* [15].

3.2   Converter theory

The easiest form of a 6-pulse converter is made up of six valves, forming a full-wave bridge circuit. It is shown in figure 4.
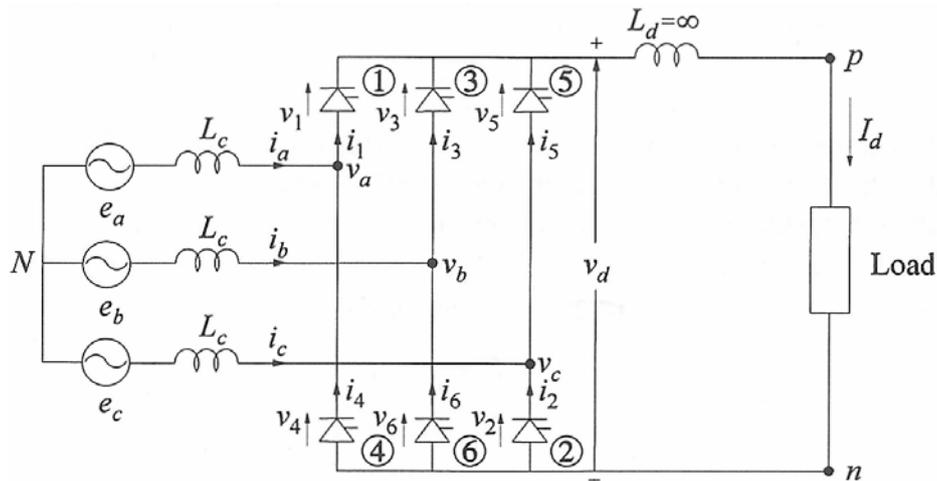

Figure 4.   A Graetz bridge [9]

The line-to-neutral voltages are:

$$e_a = E_m \cos(\omega t + 60°)$$
$$e_b = E_m \cos(\omega t - 60°)$$
$$e_c = E_m \cos(\omega t - 180°)$$

The cathodes of the three upper valves are connected. This means that when the line-to-neutral voltage of any phase is higher than the cathode voltage, that valve will conduct if the ignition delay is set to zero (mentioned soon). The other valves do not conduct at this time since they are reverse biased.

In the lower row the anodes are connected together. Here, the line-to-neutral voltage needs to be lower instead of higher for conduction to be possible.
Commutation overlap is an exception to this rule, more on this later.

The ignition delay is used to lower the DC voltage. The delay angle is denoted by α, which is equal to α / ω seconds. The valves now begin to conduct at $\omega t = \alpha$ instead of $\omega t = 0$, at $\omega t = \pi / 3 + \alpha$ instead of $\omega t = \pi / 3$, and so on, which is shown in figure 5.

11 (38)
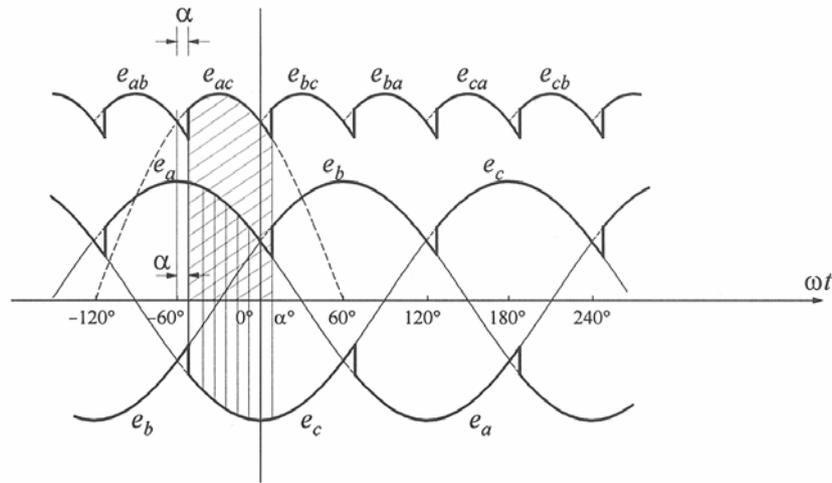
Figure 5. Ignition delay [9]

The highest value of α is 180°. If that value is exceeded, the valve cannot conduct due to reverse bias. Note valve 3 in figure 4 and phase b (e_b) in figure 5. If α>180°, the voltage potential of phase a (e_a) is higher than the voltage potential of phase b and ignition for valve 3 is impossible.

By changing α, the DC voltage V_d can become either positive or negative. A positive value corresponds to a rectifier and a negative value corresponds to an inverter. See the formula below [9].

$$V_d = V_{d0} \cdot \cos(\alpha) - R_c I_d$$

where [9]

$$R_c = \frac{3}{\pi} \omega L_c$$

V_{d0} is the ideal no-load direct voltage and $R_c I_d$ is the resulting voltage drop due to commutation overlap. Commutation overlap exists due to the inductance of the AC grid (L_c), which makes the transition of current from phase to phase take time (the current through an inductance cannot change instantly). This means that three valves will conduct during commutation, two of them forming a short-circuit. By analyzing the circuit in figure 4 during commutation (e.g. from valve 1 to 3) it can be seen that during this period the voltage at p drops to (e_a+e_b)/2 instead of e_b, which is shown in figure 6. This results in a reduction in DC voltage which is what $R_c I_d$ represented in the DC voltage formula. Note that R_c is not real resistance. It is only defined to express the voltage drop due to commutation overlap [9].

12 (38)
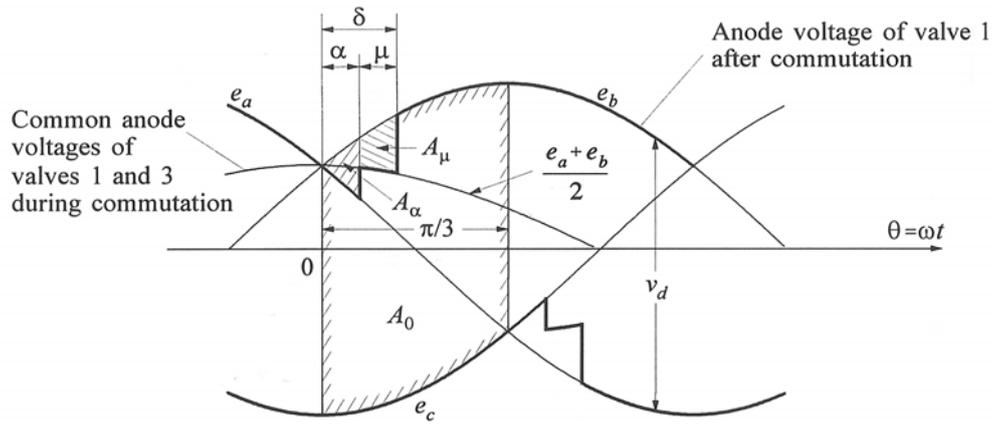
Figure 6.   Commutation overlap [9]

The commutation time expressed in rad/s (or degrees) is called overlap or commutation angle (μ), also shown in figure 6. The sum of the ignition delay α and the commutation overlap μ is called extinction delay angle (δ). Figure 7 shows this for the three AC phases. The unfiltered DC voltage is also shown in figure 7.
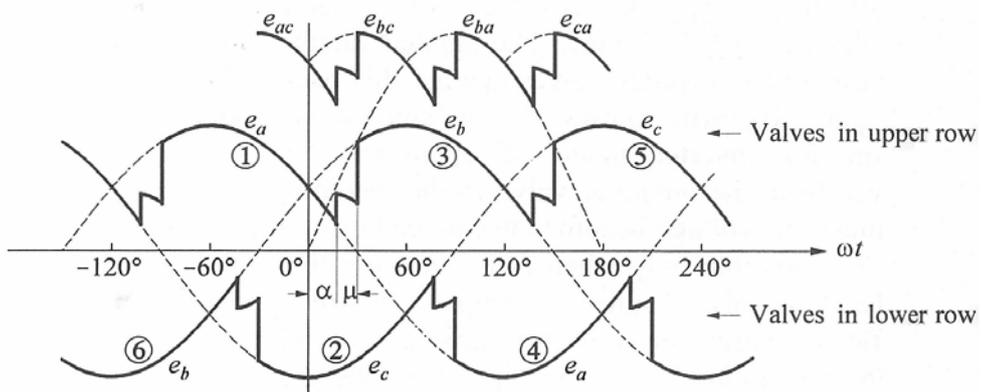

Figure 7.   Rectifier operation [9]

The terms used above are defined for rectifier operation. For inverter operation the commutation overlap is also called μ but the ignition delay is called extinction advance angle (γ) because the current is changed before in time, not after. The sum of these is called ignition advance angle (β) [9]. This can be seen in figure 8.

13 (38)
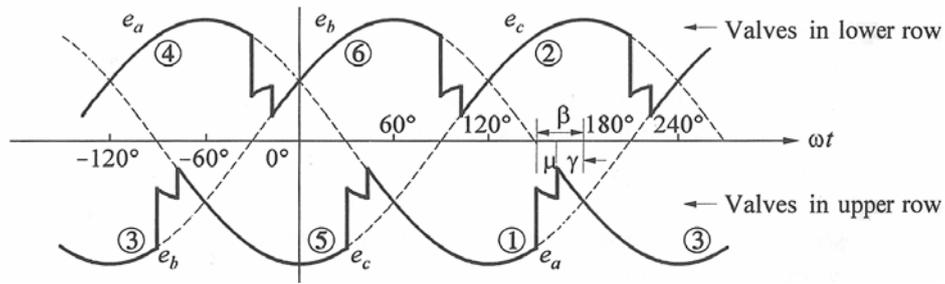
Figure 8.   Inverter operation [9]

3.3   HVDC control

The current through the HVDC link can be expressed as [9]

$$I_d = \frac{V_{d0r} \cos\alpha - V_{d0i} \cos\gamma}{R_{cr} + R_L - R_{ci}}$$

V_{d0r} is the ideal no-load direct voltage at the rectifier and V_{d0i} is the ideal no-load direct voltage at the inverter. R_{cr} and R_{ci} are the commutating resistances at the rectifier and inverter, respectively. R_L is the DC line resistance.

Thus, the DC current can be altered by changing α, γ, V_{d0r} or V_{d0i}. The first two quantities are altered by the valve gate control. Changing the tap at the converter transformer(s) alters the last two quantities, the first for the rectifier and the last for the inverter.

α and γ are rapidly changed by the valve gate control (1 – 10 ms) but to change the tap requires much more time (5 – 6 s). Rapid changes are thus made by changing α and γ. Then, the transformer tap is changed to restore α and γ to their nominal values [9].

The approximate power factor for the rectifier and inverter is [9]

$$\cos\phi \approx \frac{\cos\alpha + \cos\delta}{2}$$

and

$$\cos\phi \approx \frac{\cos\gamma + \cos\beta}{2}$$

The reactive power consumption is about 50% of the DC power. Rectifier α and inverter γ should thus be minimized to keep the converter stations' reactive power consumption as low as possible. However, to leave some room for changes in the DC voltage, α is usually set to 15° to 20° while γ is typically set to 15° to avoid commutation failure [9].

Due to the reactive power consumption, reactive power compensation is used at both converter stations. For strong grids, shunt capacitors is sufficient while SVC's or synchronous condensers might be necessary for weaker grids. In all cases the thyristor bridges need a sufficiently strong grid in terms of short-circuit capacity for commutation. If generators are located close to the converters, they can be of great help to accomplish reactive power compensation [9]. Have a look at the map of the Nordic transmission system in figure 1. Several converter stations have a power plant located in their vicinity.

An HVDC control system can be divided into four parts, from the highest to the lowest: overall system control, master control, pole control and bridge control.

The bridge control determines the α and γ limits and the valve firing instants for one bridge. The pole control converts the current order from the master control to a firing angle order and handles some protection routines. It also coordinates the bridge controls. The current order for all poles is determined by the master control. The master controller receives power flow commands from the overall system control. AC system stabilization (e.g. a POD) is also handled at the overall system control level [9].

3.4 Damping controller theory

To use an HVDC system for damping purposes is a proven method. It has been studied in e.g. [16]. The following part explains how it is done.

When a DC line is connected in parallel with one or more AC lines, the DC power can be controlled in such a way that the damping of oscillations on the AC line is increased. It works like this: The AC system frequency is measured at e.g. both converter stations. If the frequency at one of the converter stations is higher than at the other, the DC link transfers power from the station with the higher AC system frequency to the station with the lower AC system frequency. This slows the faster generator group down and makes the slower generator group run faster. This is what makes the oscillation subside faster.

The formula below describes this.

$$P_{damp} = k\Delta f$$

Since the power transfer capacity at Hasle is limited by insufficient damping, increasing the damping has the effect of increasing the maximum power transfer capacity towards the thermal limit.

This is how the principle works, but some supplementations might be needed when implementing a POD. First, the phase response should be satisfactory. Otherwise, the full potential of the POD is not utilized. Actually, the damping is lowered if the damping power is in phase with the power fluctuations present during the oscillation.

Further, a low pass filter can also be needed to make sure the POD does not begin to control frequencies that are beyond its specifications. E.g. in the IPP HVDC project, an oscillation was created due to excessive controller bandwidth [13]. Last, the output of the damping controller can be limited to avoid excessive voltage swings.

4 MODELING THE NORDIC POWER SYSTEM

This chapter describes the properties of the simulation model.

4.1 The simulation model

The simulation model received from SINTEF arrived in PSS/E 28 format. Since PSS/E was not available, Eurostag [17] was used instead. The PSS/E files were imported to Eurostag by using the data conversion program included in Eurostag. Some files were converted by hand.

The simplified HVDC model from the Eurostag model library was used for the HVDC implementation. The simplifications are described in [18]. The damping controller was also implemented. See part 4.2 for more information.

The purpose of this model is to simulate dynamic phenomena in the Nordic power system. The production is close to 50,400 MW and corresponds to a cold autumn day [6]. It consists of 22 generators and 41 buses as seen in figure 9. This figure shows how the simulation model looks in PSS/E. NO_S is southern Norway, NO_M is middle Norway, and so on.

Since the real Nordic power system is much more complex than this model, these kinds of simplifications might seem too crude. They are perfectly acceptable, though, since it's the modes and their damping that is of interest here, not load flow calculations with high accuracy. To use a simplified model is therefore a good idea since it speeds up the computation time [3, 13].
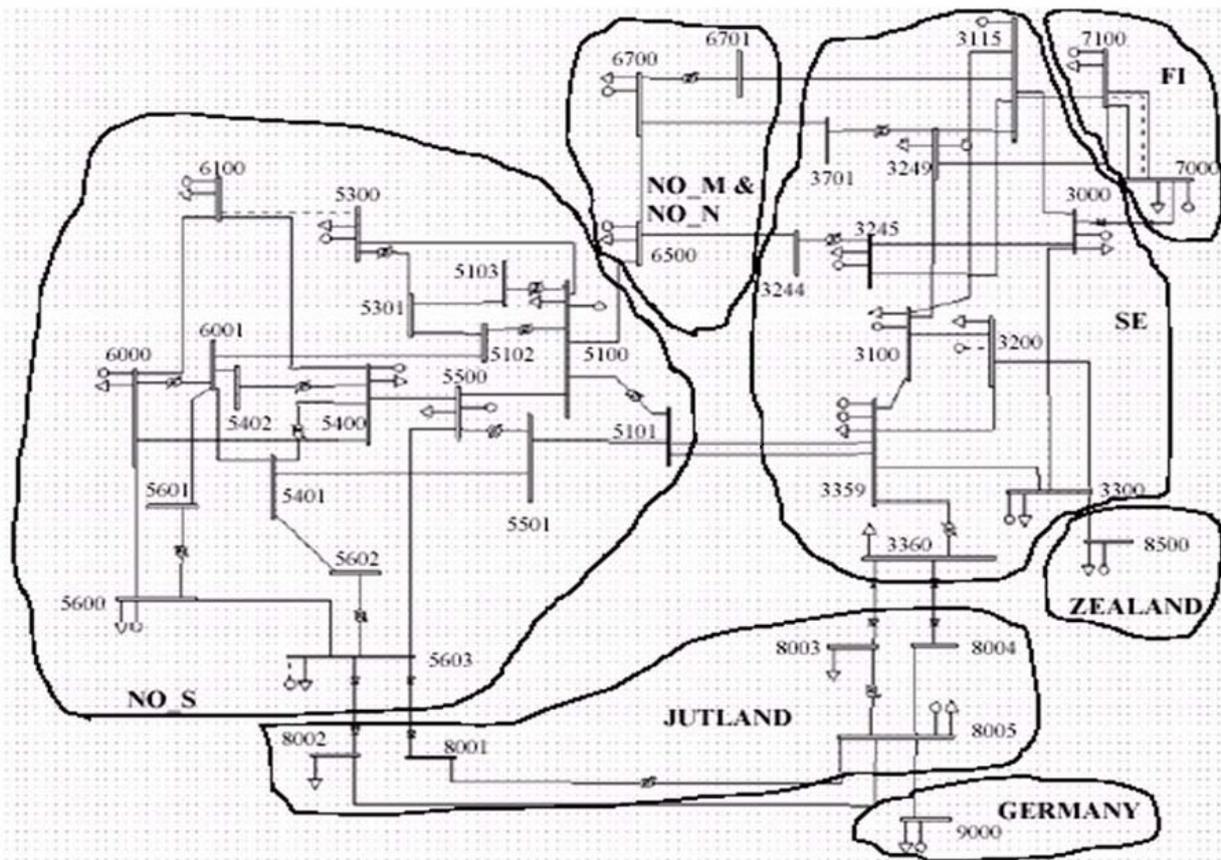
Figure 9.	The PSS/E simulation model. The Hasle lines are located between 3359 and 5101 in the center of the picture

Figure 10 is a geographical representation of the simulation model. The color of the generators indicates which country they are installed in.
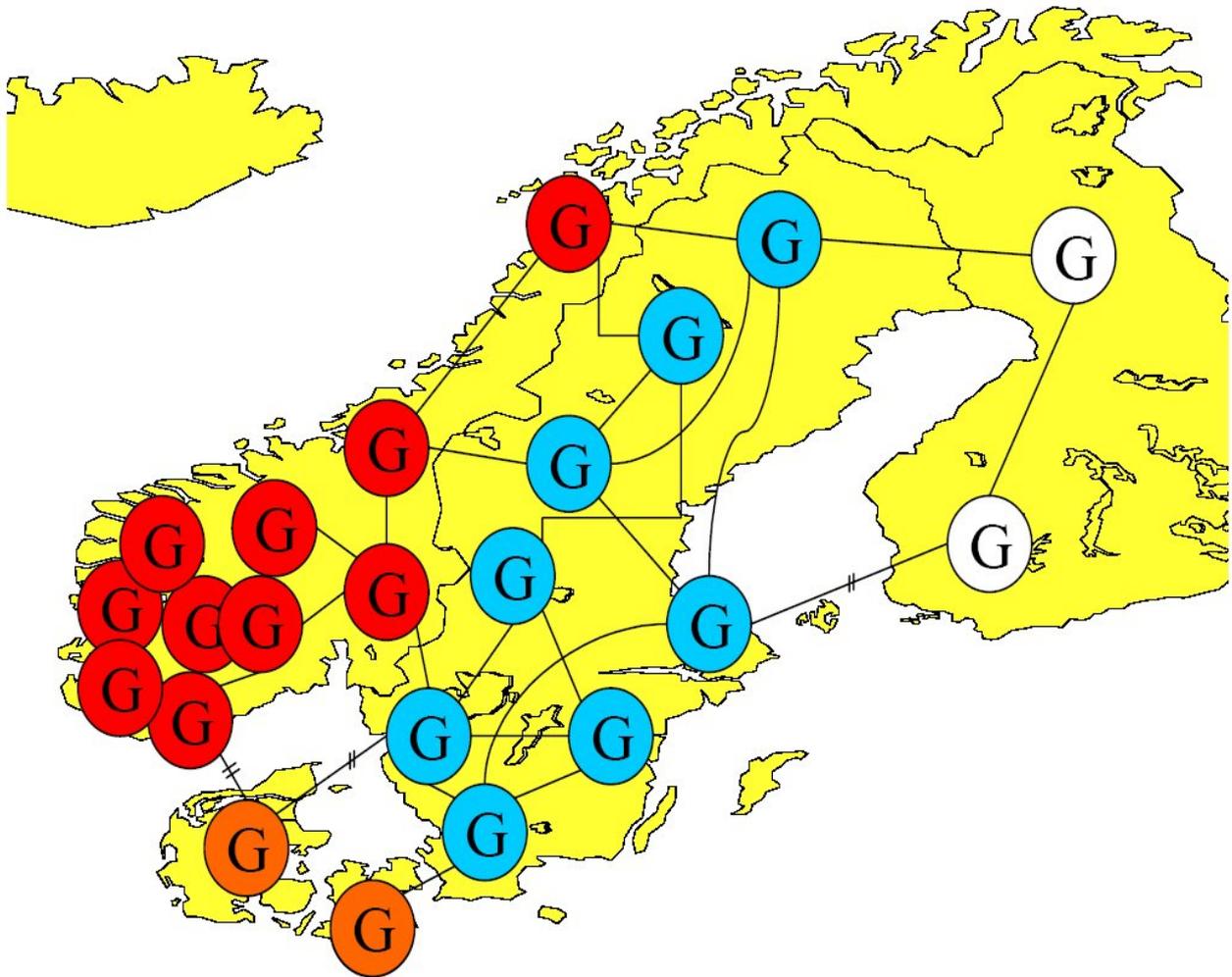
Figure 10.   A geographical representation of the simulation model [19]

4.2 HVDC implementation

An overview of the HVDC system is shown in the figure below. The blocks represent different parts of the HVDC implementation. INTERCMP is not used in this work since only small DC power transfers are used.
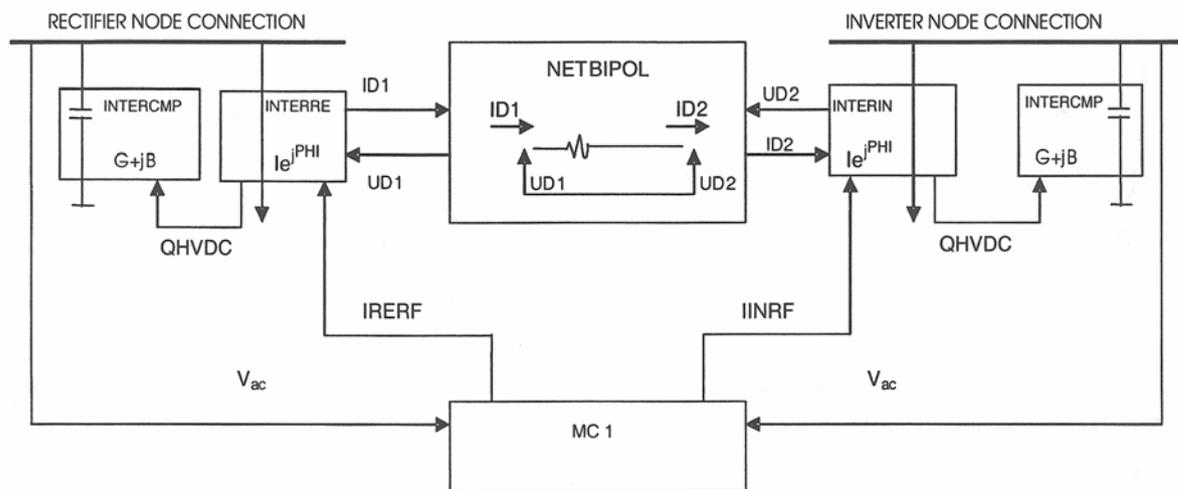
Figure 11.   Eurostag simplified HVDC model [18]

Two HVDC links were implemented. The first between 5603 and 8002 (see figure 9) and the second between 3360 and 8004. 8002 and 3360 are rectifiers and 5603 and 8004 are inverters.

Figure 12 below shows the POD implementation. The total gain is $4 \cdot 10^3$ MW/Hz.
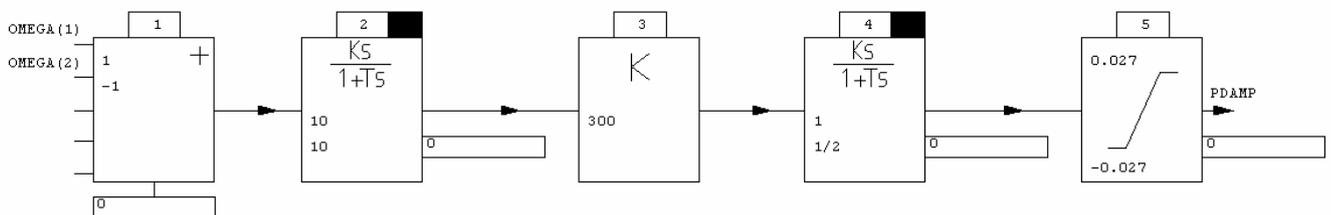
Figure 12.   The POD

The output of block 1 is the frequency difference between node 3359 and 5101, block 2 is a high pass filter, block 3 is a gain, block 4 is the phase correction and block 5 is the limiter. The gain was manually set to 300 for strong POD interaction. Too high gain results in reduced performance due to decreased damping of other modes while too

small gain results in weak POD utilization. The phase at 0.54 Hz is changed +31° by the phase correction block. The limiter is set to ±0.027, which corresponds to ±12 MW of damping power and ±2.9 kV of voltage variations at the 420 kV level in Jutland. In one case the limiter was set to ±50 MW. This corresponds to about ±12 kV voltage variations in Jutland. Also, the master controller was expanded to include the POD output. This is seen in appendix A.1.

The POD used in the Fenno-Skan HVDC link (SE – FI) can be seen in [20]. Test results from the Fenno-Skan POD implementation can be seen in [21]. This POD also uses a frequency difference as input signal.

5   SIMULATIONS

This chapter presents the results of the simulations carried out in Eurostag. Both linear and non-linear analysis is performed. The damping before and after the implementation of the POD is presented for both.

5.1   Linear analysis

Four different cases of original damping of the interarea mode at 0.54 Hz were chosen: approx. 4%, 2%, 0% and –2%. The POD was then activated and the new eigenvalues of the mode were determined. This was done in Eurostag by placing an eigenvalue computation command in the event file. The damping ratio of the mode was then calculated by using the damping ratio formula from the modal analysis chapter.

One of the Hasle lines is disconnected here to be able to compare the post-fault damping with the non-linear case. In the non-linear case a permanent short circuit and subsequent breaker openings are simulated – only one Hasle line in service after that event.

Table 1 below holds the results and includes the mode data and the damping ratio for the 0.54 Hz interarea oscillation for each of the eight different cases.

POD off		POD on	
Mode	Damping ratio (ζ)	Mode	Damping ratio (ζ)
$-0.133 \pm j3.44$	**3.9%**	$-0.882 \pm j3.44$	**25%**
$-0.0647 \pm j3.39$	**1.9%**	$-0.789 \pm j3.49$	**22%**
$0.00091 \pm j3.40$	**0.0%**	$-0.691 \pm j3.54$	**19%**
$0.0655 \pm j3.39$	**-1.9%**	$-0.594 \pm j3.58$	**16%**

Table 1.   Small-signal damping improvements

The results show very large increases in damping for all four cases.

5.2   Non-linear analysis

Placing a permanent three-phase fault on one of the Hasle lines and then disconnecting that line after 150 ms excited the interarea mode at 0.54 Hz. The circuit breakers at nodes 3359 and 5101 were used to isolate the fault.

Two different cases of short circuit impedance were chosen: 0 p.u. (0Ω) and 0.1 p.u. (176Ω) Larger oscillations should be excited in the 0 p.u. case since this kind of short circuit is the most severe, especially since it is placed on the 420 kV level.

Figure 13 shows the fault location in the Nordic transmission grid and figure 14 shows the fault location in the simulation model.
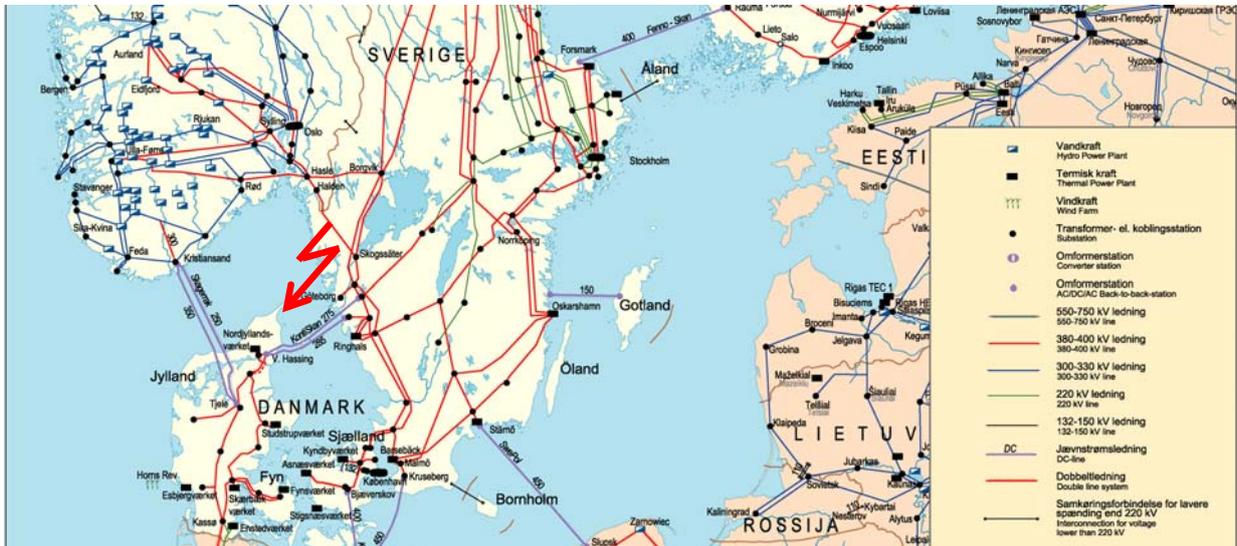

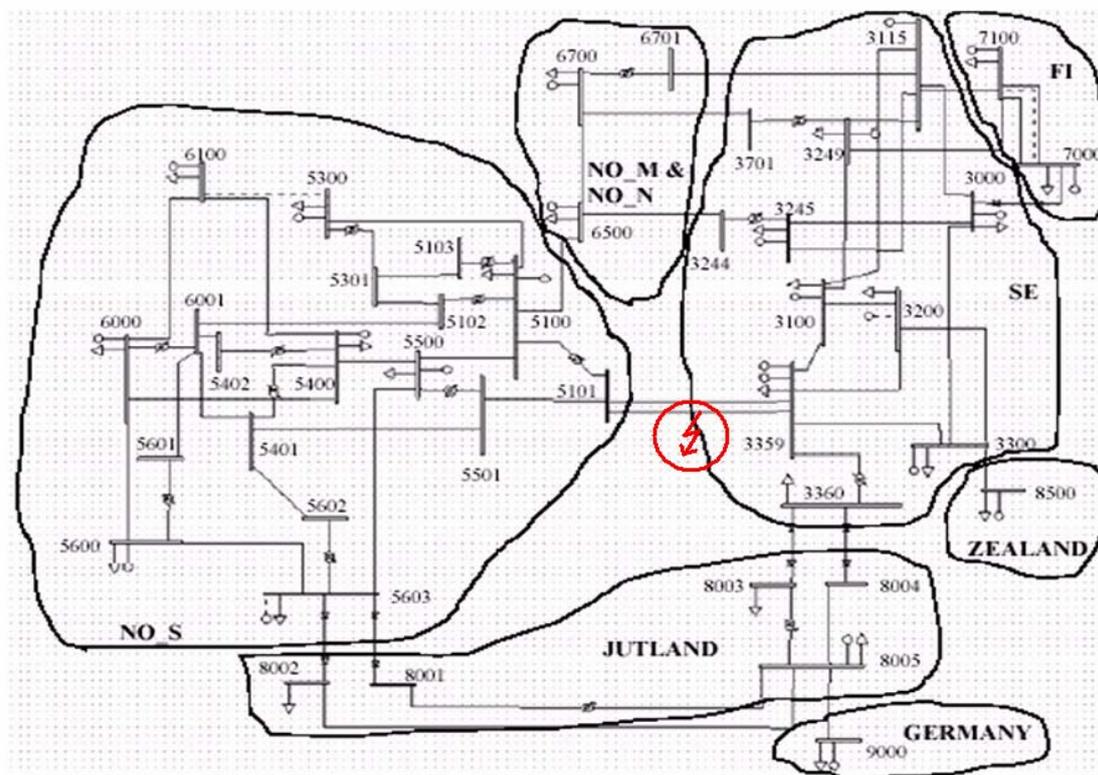Figure 13.   The fault location shown in the Nordic transmission grid [2]

Figure 14.   The fault location shown in the simulation model

During transient events such as this the linear analysis is not valid. Instead, time simulations were used to determine the damping improvement made by the POD. The four cases of different damping used in the linear case were also used here to be able to compare the results more easily. The first four simulations were without the POD and the next with POD for both cases of short circuit impedance.

Since the eigenvalue computation is not valid here the damping ratio was calculated differently. ω was set to 0.54 Hz in all cases since that is the frequency of the mode of interest. σ was found out by fitting an exponential function so that the positive oscillation envelope was under the exponential function in almost all cases. The decay of the exponential function determined the value of σ. The damping ratio could then be calculated and the results compared with the findings from the small-signal analysis.

Table 2 and 3 below show the results from the 0 p.u. case and the 0.1 p.u. case, respectively. The asterisk in table 2 indicates the case with ±50 MW damping power.

Damping ratio (ζ) at Z = 0 p.u.		
POD off	POD on	Figure
4%	9%	15
2%	7%	16
0%	3%	17
-2%	-1% / 3%*	18

Table 2.   Non-linear damping improvements for ω=0.54 Hz at Z=0 p.u. (0Ω)

Damping ratio (ζ) at Z = 0.1 p.u.		
POD off	POD on	Figure
4%	13%	19
2%	12%	20
0%	9%	21
-2%	3%	22

Table 3.   Non-linear damping improvements for ω=0.54 Hz at Z=0.1 p.u. (176Ω)

The damping is improved for all cases, though not by as much as in the linear case. See chapter 5.3 for a discussion of the results.

On the following pages the figures from the time simulations are presented with and without POD. First, the 0 p.u. case and then the 0.1 p.u. case. Please note that the y-axis

range is different and particularly that in the -2% cases it is larger since negatively damped oscillations are present there.

The result from the Fenno-Skan test is similar. With POD the damping of the oscillation is increased. See [21] for more information.
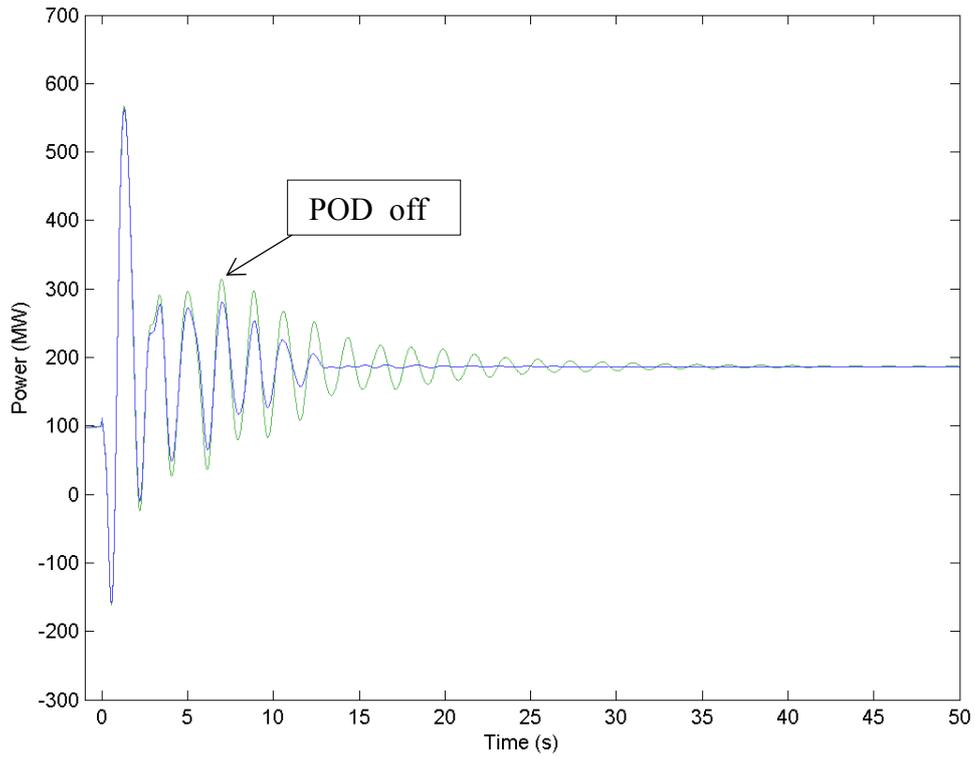
Figure 15. $\zeta_{original} = 4\%$, $Z_{fault} = 0$ p.u.

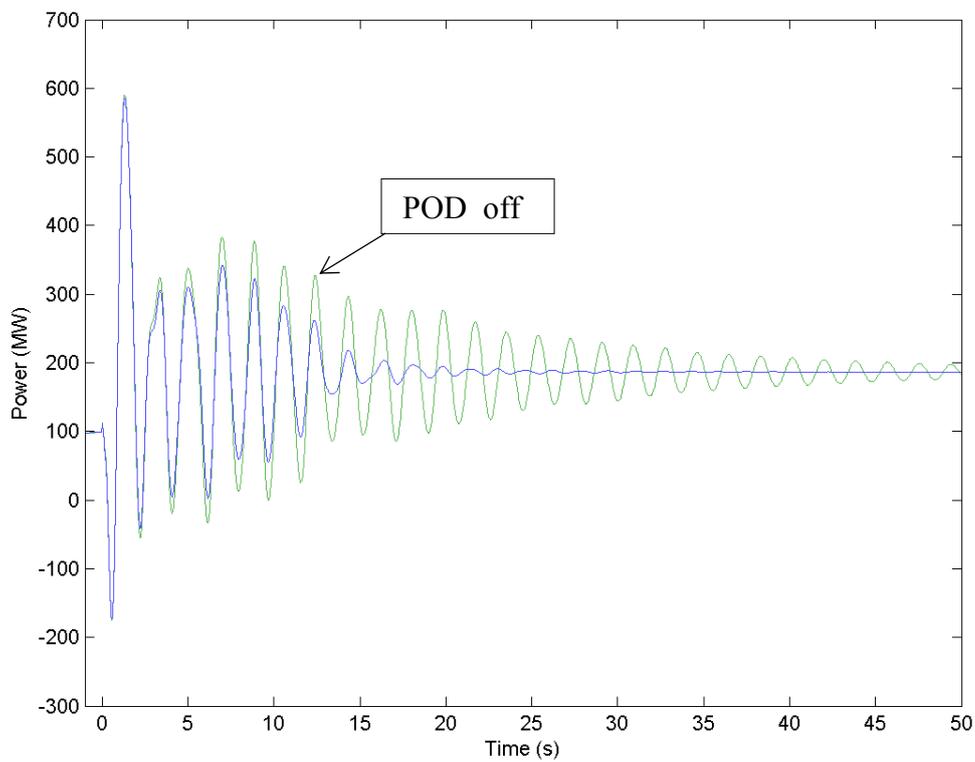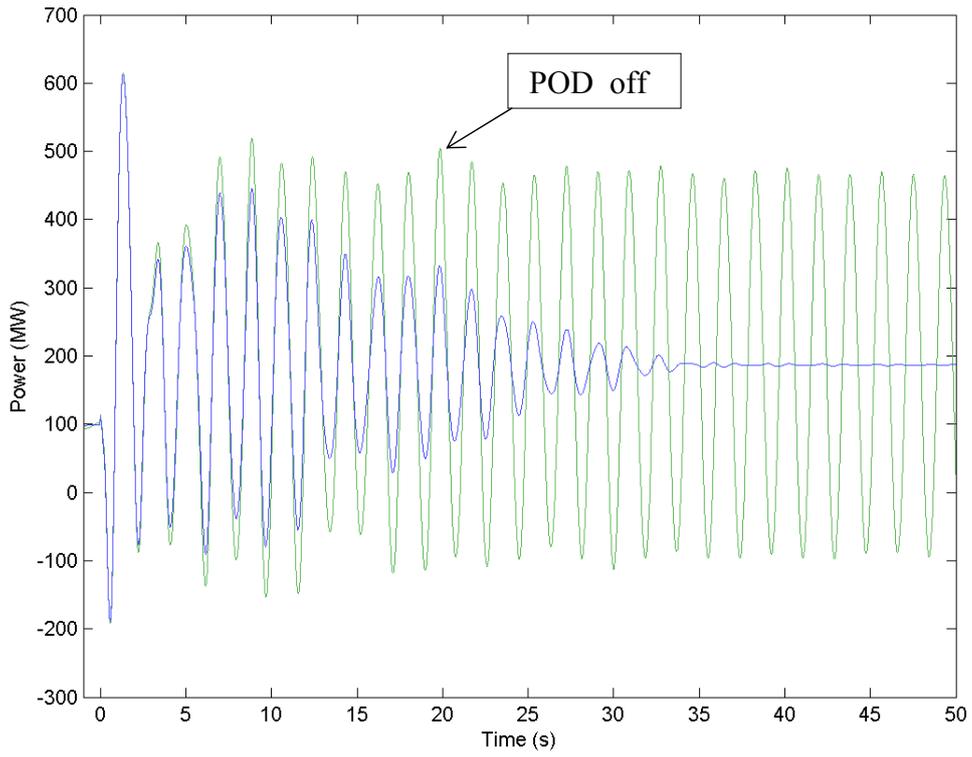Figure 16. $\zeta_{original} = 2\%$, $Z_{fault} = 0$ p.u.

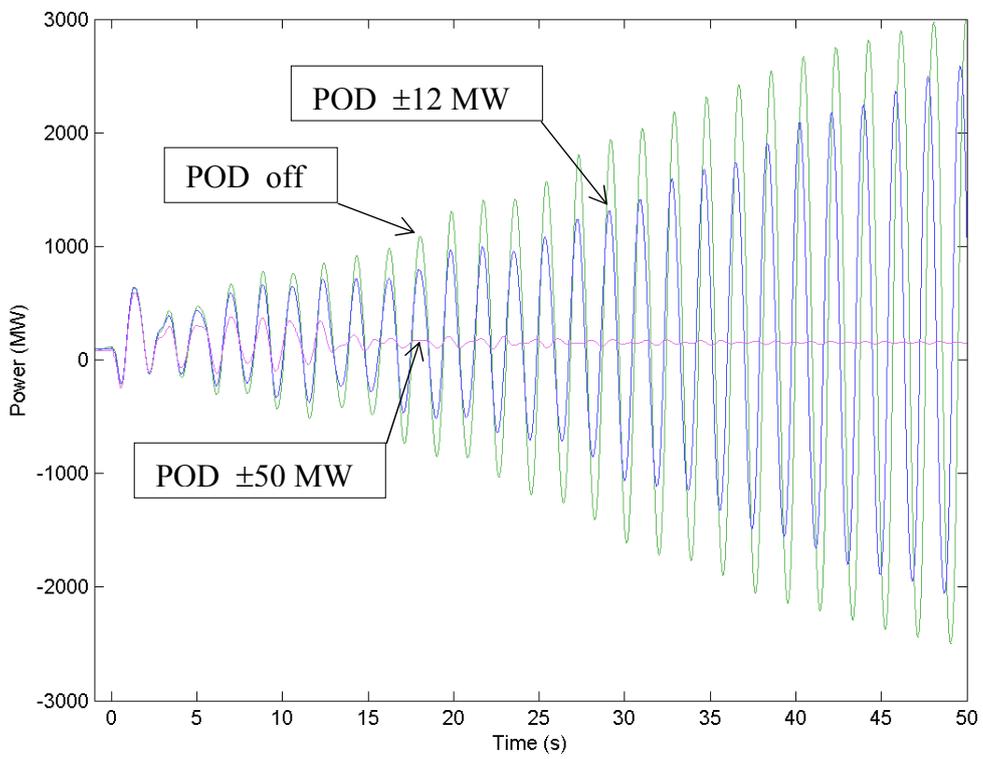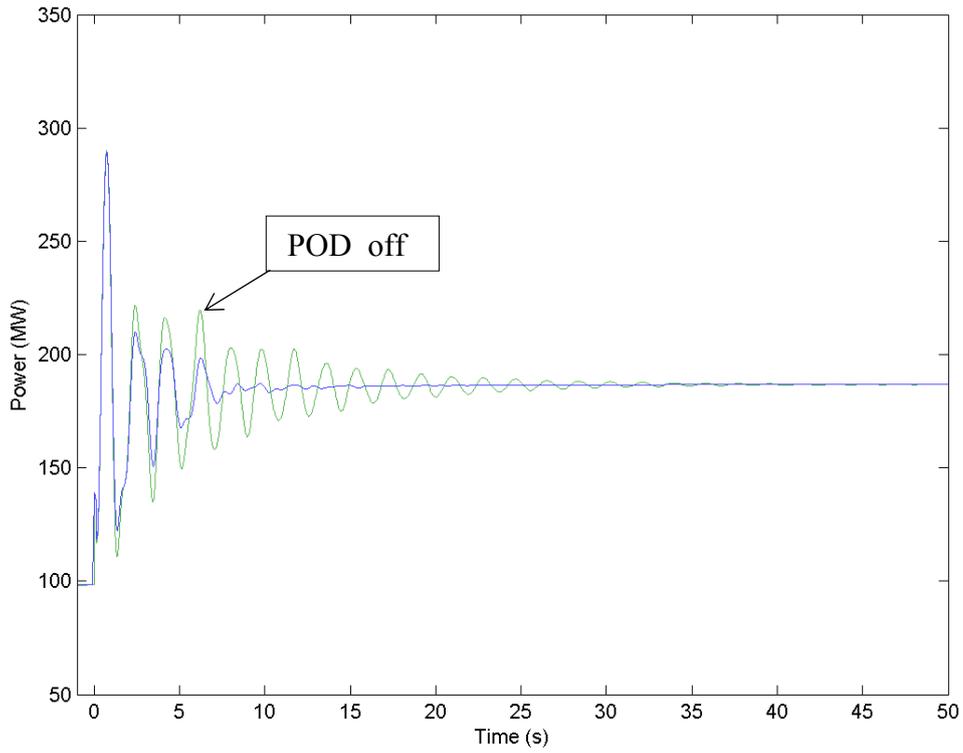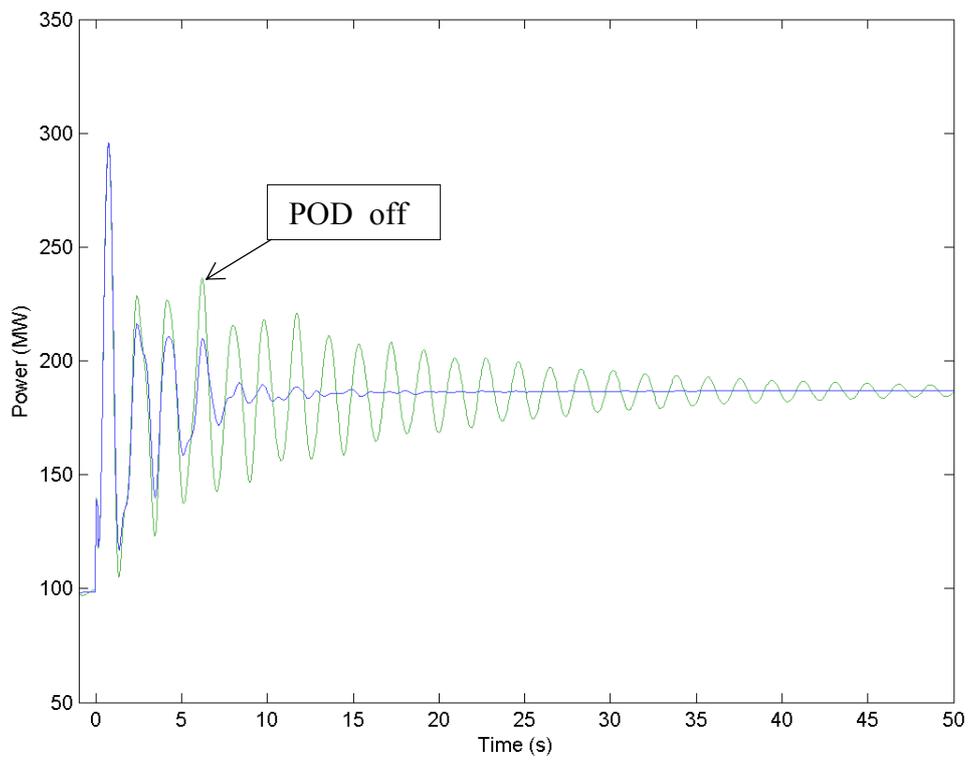Figure 17. $\zeta_{original} = 0\%$, $Z_{fault} = 0$ p.u.

Figure 18. $\zeta_{original} = -2\%$, $Z_{fault} = 0$ p.u.

Figure 19. $\zeta_{original} = 4\%$, $Z_{fault} = 0.1$ p.u.

Figure 20. $\zeta_{original} = 2\%$, $Z_{fault} = 0.1$ p.u.
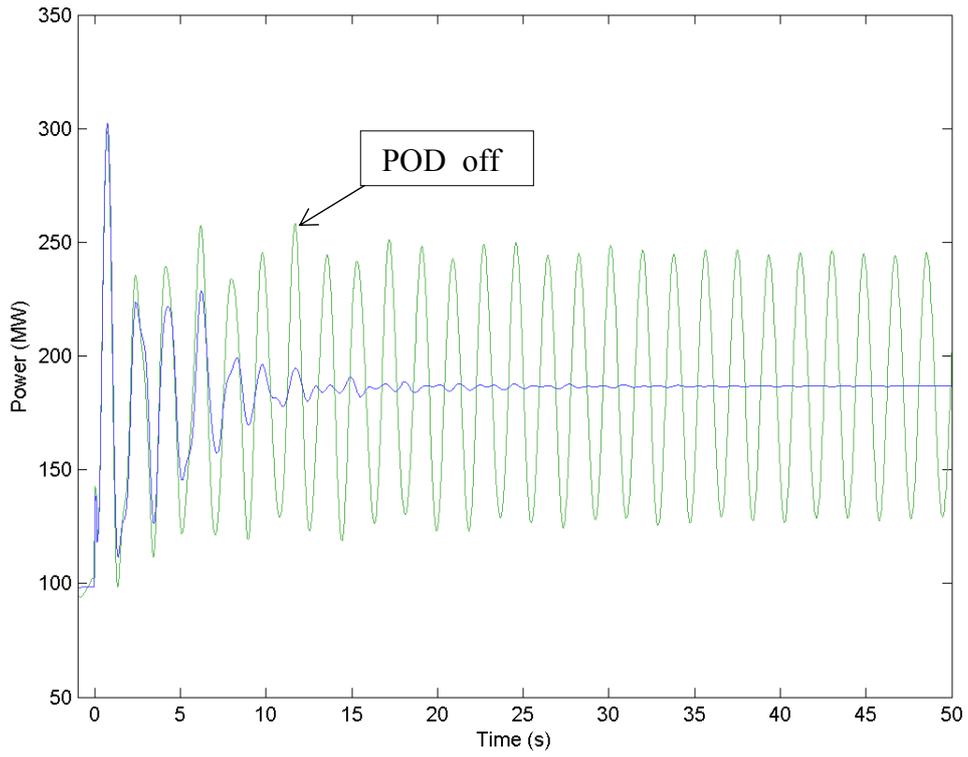
Figure 21. $\zeta_{\text{original}} = 0\%$, $Z_{\text{fault}} = 0.1$ p.u.
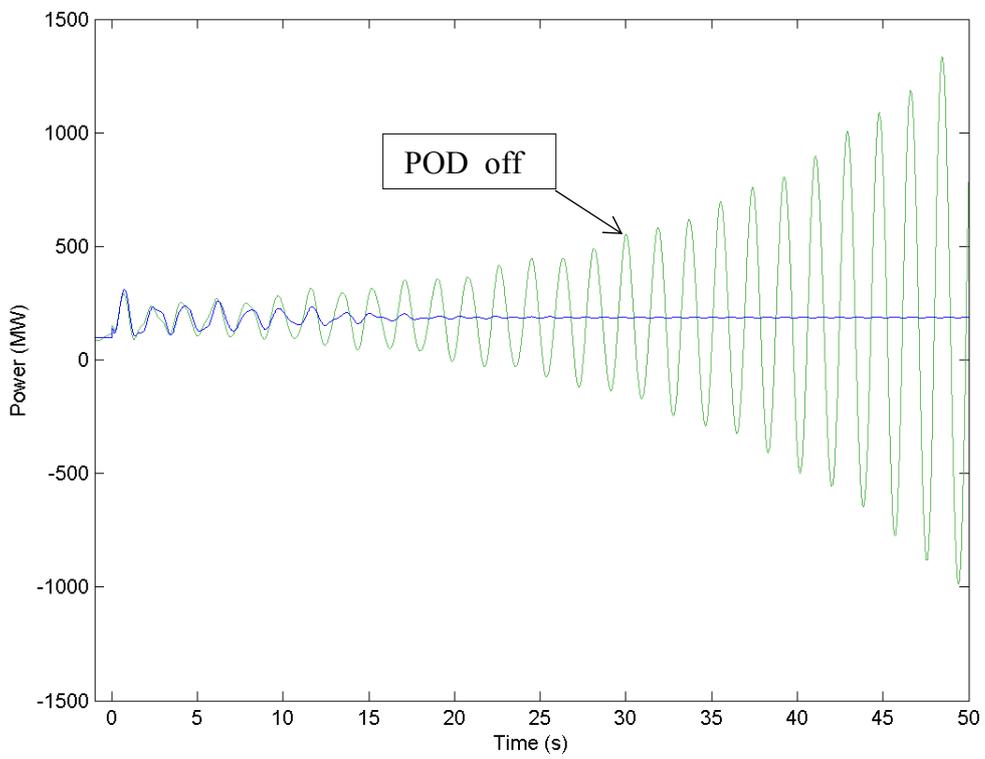
Figure 22. $\zeta_{\text{original}} = -2\%$, $Z_{\text{fault}} = 0.1$ p.u.
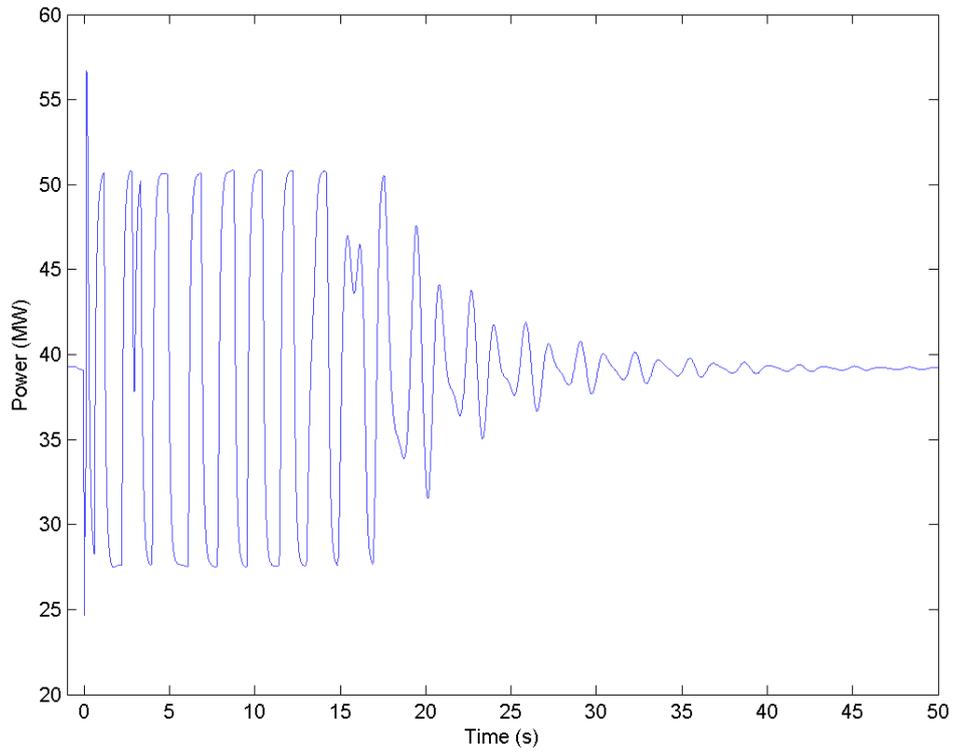
Figure 23. DC power for the converter at node 3360 (Sweden). This is for the case with $\zeta_{original}$ = 2% and Z_{fault} = 0 p.u.
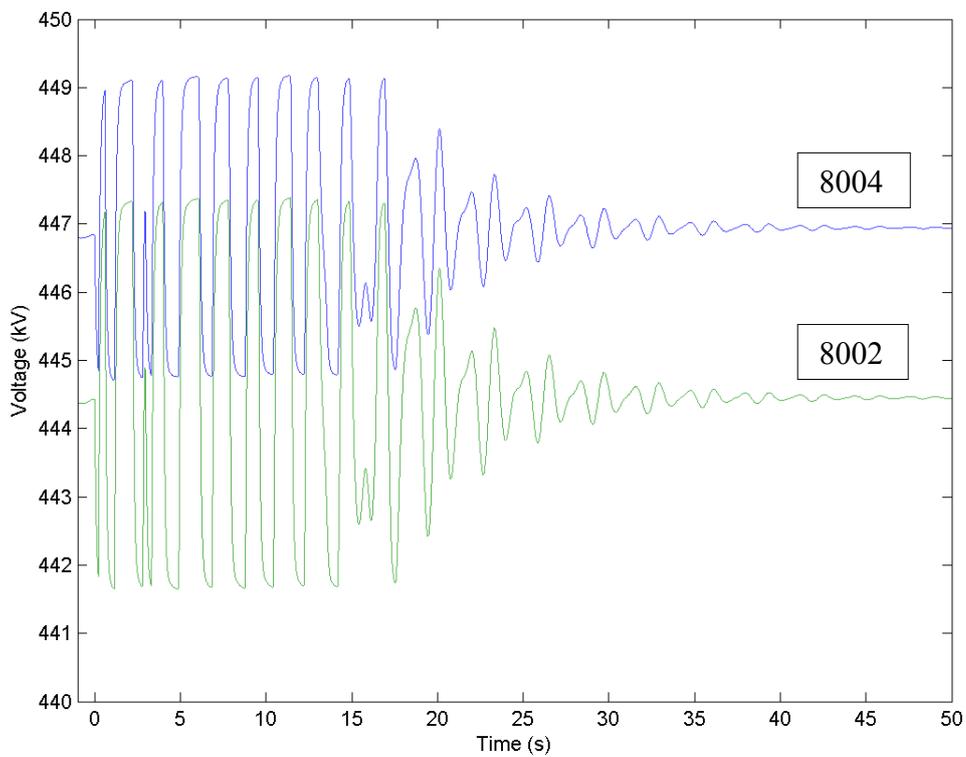
Figure 24. Voltages at nodes 8002 and 8004 (both located in Jutland). POD on.

5.3   Discussion

The damping in the small signal case is higher than in both transient cases. This shows that the linear analysis is not valid for transient disturbances, just as expected. The damping is also higher in the 0.1 p.u. case than in the 0 p.u. case. This is also to be expected because a 0 p.u. short circuit is more severe than a 0.1 p.u. short circuit – the limiter is engaged more often during a more severe event so the relative damping power reduces as the fault severity increases. For the case with -2% damping at 0 p.u. short circuit impedance the POD was able to create 3% damping when the limiter was set to ±50 MW but only -1% damping with the limiter at ±12 MW. This is because the fault was so severe that ±12 MW of damping power was not enough to create positive damping.

Also, since not all faults in a power system occur on the 420 kV level, the resulting disturbances after faults on lower voltage levels should be smaller. This will likely improve the damping results.

Thus, for normal operation or during small events, the damping improvement is excellent. For larger events, the damping improvement is good. For severe events, the damping improvement is still good, but not as good.

In all cases the improved damping comes at a cost of modulation of the 420 kV voltage in Jutland. However, this disturbance is considered small compared to the benefits provided by the increased damping.

Note that these results are valid for faults that excite the 0.54 Hz mode. See the next chapter for more information.

6   FUTURE WORK

This chapter presents some areas that could be improved if further investigation is deemed necessary.

Faults that excite other modes are likely to have different frequencies and damping. If such oscillations occur at Hasle, the damping improvement for those modes would be interesting to study. However, [6] described 0.58 Hz (0.54 Hz here) as the power transfer limiting mode at Hasle in this model, so the results should still be valid.

Finding the optimum POD limit is also interesting since high damping powers come at the cost of voltage variations in Jutland. The trade-off between these that all involved TSOs can accept remains to fix.

After the conversion from PSS/E-format to Eurostag-format the model was unstable. Tuning the generator governors rectified this. The cause of this instability should be found out or PSS/E be used instead.

The commutating resistance R_c used in the simulation model came from the Eurostag simplified model, not from Nordic data. However, different values of R_c should only change the DC voltage, which is easily rectified by the HVDC control.

To simplify the HVDC implementation, all converter stations were designed for 420 kV AC. Where the AC network was at a lower voltage level, a lossless transformer was inserted in between. This should not affect the results, though.

To further increase the accuracy the full HVDC model could be used instead of the simplified model that is used in this work.

The impact of communication delays in a real implementation should be quantified.

It would be interesting to conduct a field test of the suggested solution to determine the real-life performance of the POD.

REFERENCES

[1]   Årsstatistik 2004 (Annual statistics 2004). Nordel 2005.
        http://www.nordel.org/Content/Default.asp?PageID=157

[2]   The Transmission Grid in the Nordic Countries (small version) – JPEG.
        Nordel 2004. http://www.nordel.org/Content/Default.asp?PageID=125

[3]   Kjetil Uhlen et al. Raising Stability Limits in the Nordic Power Transmission
        System. 14th PSCC, Sevilla, 24-28 June 2002. Session 30, Paper 3, Page 1.
        www.eeh.ee.ethz.ch/pscc02/papers/s30p03.pdf

[4]   Svenska Kraftnät, Nätteknik, Jan Halvarson. Utbyggnad av Fenno-Skan.
        Protokoll 2005-10-12.
        www.svk.se/upload/4166/Protkoll_Samrad_lsty_mfl_tidigt_20050428.pdf

[5]   Prioritised Cross-Sections Reinforcement Measures within the Nordic
        Countries – Status June 2005. Bilaga 7 Nordel styrelsemöte 13 juni 2005.
        Nordel 2005. www.nordel.org/Content/Default.asp?PageID=129

[6]   Espen Hagstrøm, Ian Norheim, Kjetil Uhlen. Large Scale Wind Power
        Integration in Norway and Effect on Damping in the Nordic Grid.
        www.elkraft.chalmers.se/Publikationer/EMKE.publ/NWPC04/papers/HAGST
        ROM.PDF

[7]   ABB HVDC. www.abb.com/hvdc

[8]   M. Klein, G.J. Rogers, P. Kundur. A Fundamental Study of Inter-area
        Oscillations in Power Systems. Transactions on Power Systems, Vol. 6, No. 3,
        August 1991. www.ee.iastate.edu/~jdm/ee554/kundur_fundamental_study.pdf

[9]   P. Kundur. Power System Stability and Control, ISBN 0-07-035958-X,
        McGraw-Hill, 1993.

[10]   A. R. Katančević. Electromechanical Oscillations and Advanced Protection
        Applications – Summary. www.hut.fi/~katale/docs/akabbchreport.pdf

[11]   O. Samuelsson. Power System Damping. Structural Aspects of Controlling
        Active Power, ISBN 91-88934-05-5, IEA, Lund University, Sweden, 1997.

[12]   O. I. Elgerd. Electric Energy Systems Theory, 2nd ed. McGraw-Hill, 1982.

[13]   CIGRE Technical Brochure on Control of Power System Oscillations, Prepared by Task Force 07 of Advisory Group 01 of Study Committee 38, Final Report as Submitted to SC38 for Review, July 1996.

[14]   Systemdriftsavtalet uppdaterat 2005. Nordel 2006. www.nordel.org/Content/Default.asp?PageID=130

[15]   Bonneville Power Administration, Transmission, CIGRE SC14, Compendium of HVDC Schemes throughout the World. Working Group 14.04, Convener: Mr. D. J. Christofersen. Task Force 14.04.02, Convener: Mr. P-O Lindh. Konti-Skan. www.transmission.bpa.gov/cigresc14/Compendium/KONTI.htm

[16]   J. Arroyo L., A. R. Messina, J. H. López, D. Olguín S. Damping of Low-Frequency Oscillations in Longitudinal Power Systems Using HVDC Modulation and SVCs. wwweurostag.epfl.ch/users_club/newsletter/PDF/HVDC.pdf

[17]   Eurostag - Home Page. www.eurostag.be

[18]   Eurostag Package Documentation part 1, Release 4.3, 2004.

[19]   Prosjektplan. Økt utnyttelse av kraftsystemet i Norden, SINTEF Energiforskning AS. Revised 2003.

[20]   L. Pottonen, R. Hirvonen, K. Jääskeläinen, M. Vaitomaa. Network Interaction Tests of the Fenno-Skan HVDC Link. IEE Fifth International Conference on AC and DC Power Transmission 17-20 September, 1991, London.

[21]   Liisa Pottonen, Ritva Hirvonen, Per-Erik Björklund. Performance Analysis of the Fenno-Skan HVDC link during network faults. CIGRE, 1996, Session Paper, Ref. No. 14-303.

A APPENDIX

A.1 HVDC system macro block

The modified part of the master controller is shown here. Block 23 is added, the two other blocks were part of the standard model. The rectifier and inverter macro blocks were not modified.
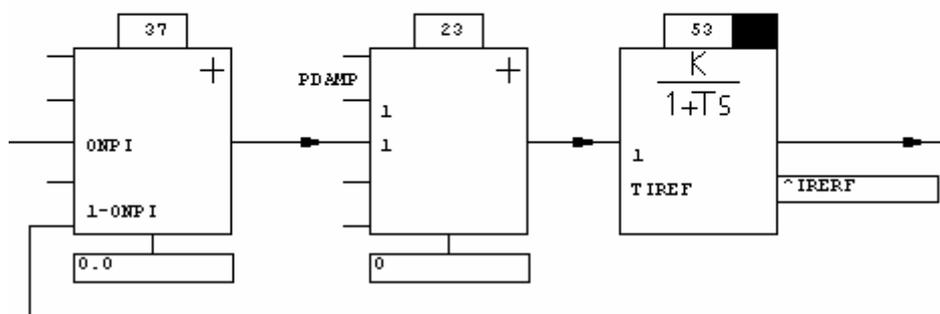

Figure A.1 The modified part of the master controller

A.2 HVDC parameters

The following table lists the parameters for the rectifier (INTER**RE**) and inverter (INTER**IN**) macro blocks that were changed from their standard values.

Parameter	Description	INTERRE*/ INTERIN
UDCBASE	DC system base voltage (kV)	299.81 kV
UDCNOM	Nominal DC system voltage (kV)	300 kV
IDCBASE	DC system base current (kA)	0.33333 kA
IDCNOM	Nominal DC system current (kA)	1.8333 kA
UCONV	Nominal converter transformer voltage on valve side (kV)	300 kV
UCONVB	Converter transformer base voltage on valve side (kV)	300 kV
VHTINI	Initial converter transformer voltage on network side (kV)	420 kV
VHTNBASE	Converter transformer base voltage on network side (kV)	420 kV
VHTNMAX	Maximum converter transformer voltage on network side (kV)	480 kV
VHTNMIN	Minimum converter transformer voltage on network side (kV)	380 kV
RL	DC line resistance (Ω)	2 Ω

Table A.1   Parameters for the rectifier and inverter. *RL is not included in INTERRE

Next, the parameters for the master controller. Only the parameters that were changed are listed here. The master controller is called MC1mod because the original master controller was modified to include the POD output signal.

Parameter	Description	MC1mod
URECNOM	Nominal rectifier DC voltage (kV)	300 kV
IRECNOM	Nominal rectifier DC current (kA)	1.8333 kA
IINVNOM	Nominal converter transformer current on valve side (kA)	1.8333 kA

Table A.2   Parameters for the modified master controller

Last, some DC line and initial parameters. Here, all were changed.

Parameter	Description	NETBIPOL
ID10	Initial DC current (kA)	0.1665 kA*
IDCBASE	DC system base current (kA)	0.33333 kA
RL	DC link resistance (Ω)	2 Ω
UD10	Initial DC voltage (kV)	294 kV **
UDCBASE	DC system base voltage (kV)	299.81 kV

Table A.3   Parameters for NETBIPOL.

*   Set to 0.3326 kA in the ±50 MW case.

**   The model did not work at 300 kV. Lowered to 294 kV in the ±12 MW cases and 290 kV in the ±50 MW case.

Figure A.2 and A.3 show the rectifier and inverter data, respectively.

Figure A.2   Rectifier data

The power operating point was set to 100 MW in the ±50 MW POD case to avoid power fluctuations too close to zero.

Figure A.3   Inverter data